Analysis of Mode Transitions in Biological Networks

Nael H. El-Farra, Adiwinata Gani, and Panagiotis D. Christofides
Dept. of Chemical Engineering, University of California, Los Angeles, CA 90095

DOI 10.1002/aic.10499
Published online May 31, 2005 in Wiley InterScience (www.interscience.wiley.com).

This work presents a methodology for the analysis of mode transitions in biological networks. The proposed approach is predicated on the notion of orchestrating switching between the domains of attraction of the steady states of the constituent modes. Initially, the overall network is modeled as a switched nonlinear system that consists of multiple modes, each governed by a set of continuous-time differential equations. The transitions between the continuous modes are triggered by discrete events (changes in model parameters that correspond to alterations in physiological conditions). Then, following the characterization of the steady-state behavior of each mode, Lyapunov techniques are used to characterize the domains of attraction of the steady states. Finally, by analyzing how the domains of attraction of the various modes overlap with one other, a switching rule is derived to determine when, and if, a given mode transition at a given time results in the desired steady-state behavior. The proposed method is demonstrated using models of biological networks that arise in cell cycle regulation and the bacteriophage λ-switch system. © 2005 American Institute of Chemical Engineers *AIChE J,* 51: 2220–2234, 2005
Keywords: switched nonlinear systems, domains of attraction, biological networks

Introduction

In a biological cell, cellular functions—such as metabolism, DNA synthesis, movement, and information processing—are implemented and controlled by vast arrays of complex networks of biochemical interactions. Understanding how these networks are integrated and regulated, and how the regulation may be influenced, possibly for therapeutic purposes, is a major goal of molecular cell biologists and bioengineers. Although experimental techniques have been, and will continue to be, an indispensable tool in the quest for such an understanding, it is now clear that the sheer complexity of biological networks is such that informal biochemical intuition alone cannot reliably deduce the underlying logic of these networks. This intuition must be supplemented by precise mathematical and computational tools that can provide both qualitative and quantitative insights into the description, analysis, and manipulation of biological networks underlying basic cellular function. From a practical perspective, such techniques could potentially reduce the degree of trial-and-error experimentation. More importantly, computational and theoretical approaches can lead to testable predictions regarding the current understanding of biological networks, which can serve as the basis for revising existing hypotheses. These realizations, together with recent technological advances that are increasingly enabling experimental validation of theoretical predictions, have been major driving forces behind a large and growing body of research work, in recent years, on the development and application of analytical and computational tools for the modeling and simulation,[1-7] optimization,[8,9] and identification[10] of biological networks. The reader may also refer to the available review papers[5,11-13] and the references therein for further results on biological networks.

Biological networks are intrinsically dynamical systems, driving the adaptive responses of a cell in space and time. The behavior of these dynamical systems is determined by "biochemical kinetics," or rate equations, in which the variables of

Current address of N. H. El-Farra: Dept. of Chemical Engineering and Material Science, University of California, Davis, CA 95616; e-mail: nhelfarra@ucdavis.edu
Correspondence concerning this article should be addressed to P. D. Christofides at pdc@seas.ucla.edu.

interest are the concentrations of individual network components (proteins, metabolites, etc.) within the cell, and the dynamics describe the rates of production and decay of these components. The dynamic models of biological networks typically consist of systems of nonlinear ordinary differential equations, permitting the modeler to apply the analytical techniques of nonlinear dynamics. These techniques have been substantially developed in recent decades, making the rate-equation approach a promising avenue for combining mathematical analysis and computational simulation.

Although the resulting models are typically based on purely continuous dynamics, the dynamics of biological networks often involve switching between many qualitatively different modes of behavior. At the molecular level, for example, the fundamental process of inhibitor proteins turning off the transcription of genes by RNA polymerase reflects a switch between two continuous processes. An example of this is the classic genetic switch observed in the bacteriophage λ,[14-16] where two distinct behaviors, lysis and lysogeny, each with different mathematical models, are seen. Also, at the cellular level, the cell growth and division in a eukaryotic cell is usually described as a sequence of four processes, each being a continuous process that is triggered by a set of conditions or events.[17-19] At the intercellular level, cell differentiation can also be viewed as a switched system.[20] In addition to naturally occurring switches, switched dynamics can be the result of external intervention that attempts to reengineer a given network by turning on or off, for example, certain pathways. In all of these examples, the overall behavior of the network is more appropriately viewed as a switched system, that is, intervals of continuous dynamics interspersed by discrete transitions, and thus a hybrid approach that combines elements of discrete and continuous dynamics is necessary, not only for the modeling, simulation, and analysis,[21,22] but also for controlling and modifying the network behavior.

Hybrid system models are increasingly being used to represent a diverse array of engineering systems, such as automotive and chemical process control systems. A hybrid system consists of a finite family of continuous dynamical subsystems (or modes), each of which is governed by a different set of differential equations, together with a set of discrete events (or logic-based switching rules) that orchestrate the transition between the constituent modes. Research on hybrid systems, both within control systems theory and computer science, has led to the development of systematic tools for the modeling,[23,24] simulation,[24] optimization,[25-27] stability analysis,[28-30] and control[31-35] of several classes of hybrid systems. Given the similarity that many biological networks exhibit to switched systems encountered in engineering (such as involving feedback mechanisms and switching), it is instructive to investigate how all these tools can be applied to model, analyze, and possibly modify the dynamics of biological networks.

Changes in network dynamics can result from alterations in local conditions (such as temperature, nutrient and energy sources, light, cell density) and/or changes in the molecular environment of individual regulatory components (such as intracellular concentrations of transcription factors). Often, the network can be switched between different modes by changes in parameter values. These parameters typically include rate constants and total enzyme concentrations that are under genetic control. Changing the expression of certain genes will change the parameter values of the model and move the network across bifurcation boundaries into regions of qualitatively different behavior (such as transitions from limit cycles to single and multiple steady states). Understanding and analyzing the nature of these qualitatively different modes of behavior typically involves bifurcation analysis, which determines how the attractors of the vector field depend on parameter values, leading to a characterization of the regions in parameter space where the different behaviors are observed. The boundaries of these regions represent the bifurcation boundaries.

An important question, however, that is not addressed by bifurcation analysis is that of when, or where, in the state space, is a transition from one mode to another feasible. For example, bifurcations can predict that a change in a certain parameter is required for the network to move from an oscillatory mode (stable limit cycle) to a multistable mode (multiple stable steady states) but cannot tell us when, or which, of the new steady states will be observed upon switching. This is an important consideration when one tries to manipulate the network behavior to achieve a certain desirable behavior or steady state. To address this question, bifurcations must be complemented by a dynamical analysis of the transient behavior of the constituent modes of the overall network. Intuitively, one expects that the newly switched mode will exhibit the desired steady state if, at the time of switching, the network state is in the vicinity of that steady state. A precise concept from nonlinear dynamical systems theory that quantifies this closeness is that of the domain of attraction, which is the set of all points in the state space, starting from where the trajectories of the dynamical system converge to a given equilibrium state.

In this work, we present a methodology for the dynamic analysis of mode transitions in biological networks. The proposed approach is based on the notion (introduced in El-Farra and Christofides[35,36]) of coupling the switching logic to the domains of attraction of the constituent modes. To this end, we initially model the overall network as a switched nonlinear system that dwells in multiple modes, each governed by a set of continuous-time differential equations. The transition between the continuous modes is triggered by discrete events (changes in model parameters that correspond to alterations in physiological conditions). Then, following the characterization of the steady-state behavior of each mode, Lyapunov techniques are used to characterize the domains of attraction of the steady states. Finally, by analyzing how the domains of attraction of the various modes overlap with one other, it is possible to determine when, and if, a given steady-state behavior, for a given mode transition, is feasible or not. The proposed method is demonstrated using models of biological networks that arise in cell cycle regulation and the bacteriophage λ-switch system.

A Switched System Representation of Biological Networks

We consider biological networks modeled by systems of nonlinear ordinary differential equations of the general form:

$$\frac{dx(t)}{dt} = f_{i(t)}(x(t), p_{i(t)}) \qquad i(t) \in \mathcal{I} = \{1, \ldots, N\} \quad (1)$$

where $x = [x_1\ x_2\ \cdots\ x_n]^T \in \mathbb{R}^n$ is the vector of continuous state variables (such as concentrations of the various network

components such as proteins, genes, metabolites, etc.), $f_i(\cdot)$ is a smooth nonlinear function, p_i is a vector of network parameters (such as kinetic constants, total enzyme concentrations) that are typically under genetic control, $i : [0, \infty) \rightarrow \mathcal{I}$ is the switching signal that is assumed to be a piecewise continuous (from the right) function of time, that is, $i(t_k) = \lim_{t \rightarrow t_k^+} i(t)$ for all $t_k \geq 0, k \in Z_+$, where Z_+ is the set of positive integers and t_k is the kth switching time, implying that only a finite number of switches occurs on any finite interval of time. N is the number of modes of the switched system $i(t)$, which takes different values in the finite index set, $\mathcal{I}$, represents a discrete state that indexes the vector field $f_i(\cdot)$, which determines $\dot{x}$. For each value that i takes in $\mathcal{I}$, the temporal evolution of the continuous state is governed by a different set of differential equations. The system of Eq. 1 is therefore a switched (multimodal) system that consists of a finite family of continuous nonlinear subsystems (modes) and a switching rule that orchestrates the transitions between them. In biological networks, mode transitions can be the result of a fundamental change in the vector field itself (such as different modes having different f_i values) or, more commonly, a change in network parameter values arising from changes in levels of gene expression and enzyme activities (which can occur spontaneously or be induced externally).

The basic problem that we address in this work is that of determining when (or where in the state space) can a transition from one mode to another produce a certain desired behavior that exists in the target mode (such as a desired steady state). From the perspective of analysis, the answer to this question sheds light on why certain naturally occurring mode transitions always seem to favor a certain steady-state behavior. From a control standpoint, on the other hand, the answer provides insight into how and when the designer should enforce the transition to bring about a desired steady-state behavior. In the next section, we outline a methodology that addresses these questions.

Methodology for Analysis of Mode Transitions

The methodology proposed here is based on the idea of designing the switching logic on the basis of the domains of attraction of the constituent modes, which was introduced in El-Farra and Christofides[35] in the context of constrained control of switched nonlinear systems. However, unlike the results in El-Farra and Christofides,[35] where the restrictions on the size of the domains of attraction were a consequence of the constraints imposed on the manipulated input of each mode, the domains of attraction considered here are directly linked to the intrinsic dynamic behavior of the constituent modes, which is dictated by the dependency of the attractors of the vector field on the network parameters. For example, the presence of multiple equilibrium points in a given mode gives rise to multiple stability regions, or domains of attraction, whose union covers the entire state space. Clearly, which equilibrium state is attained depends on which region contains the system state at the switching time. Below is the proposed methodology:

(1) Identify the different modes of the network, where each mode is characterized either by a different set of differential equations or by the same set of equations but with different parameters.

(2) Compute the steady state(s) of each mode by solving:

$$0 = f_i(x_s, p_i) \tag{2}$$

where x_s is an admissible steady-state solution. Depending on the values of p, each mode might possess a limit cycle, a single steady state, or multiple steady states.

(3) Characterize the domain of attraction (stability region) of each steady state in each mode. For a given steady state, x_s, the domain of attraction, $\Omega(x_s)$, consists of the set of all states starting from where the system trajectories converge to that steady state. Estimates of the domain of attraction can be obtained using Lyapunov techniques.[37] For example, consider the case of isolated equilibrium points and let V_i be a Lyapunov function candidate, that is, $V_i(x_s) = 0$ and $V_i(x) > 0$ for all $x \neq x_s$. Consider also the set $\Pi(x_s) = \{x \in \mathbb{R}^n : \dot{V}_i(x) < 0\}$. Then the level set, $\Omega(x_s) = \{x \in \mathbb{R}^n : V_i(x) \leq c_i^{max}\}$, where $c_i^{max} > 0$ is the largest constant for which Ω is fully contained in Π, provides an estimate of the domain of attraction of x_s (see El-Farra and Christfides[38,39] for more details on this issue). Because of the possible conservatism of the resulting estimates, Lyapunov techniques are usually coupled with other methods to obtain larger estimates (such as multiple Lyapunov functions; see chapter 4 in Khalil[37] for details).

(4) Analyze how the domains of attraction of a given mode overlap with those of another mode. Suppose, for example, that the network is initialized within mode k and let T be the transition time from mode k to mode j. Also, let x_s be an admissible steady state (among several others) of the jth mode. Then, if

$$x(T) \in \Omega_j(x_s) \tag{3}$$

and $i(t) = j \; \forall \; t \geq T^+$ (that is, no further switches take place), then we will have $\lim_{t \rightarrow \infty} x(t) = x_s$, that is, the x_s steady state will be observed after switching. The switching rule of Eq. 3 requires monitoring the temporal evolution of the state evolution to locate where the state is at the switching time, with respect to the domains of attraction of the mode to be activated.

Remark 1. Referring to the computation of the steady states of a biological network, we note that it is, in general, difficult to compute all the steady-state solutions of a system of nonlinear ordinary differential equations (ODEs). For an arbitrary system of nonlinear ODEs, where the right-hand side does not possess any kind of structure, one can resort to general search algorithms, such as Newton-type methods, to solve Eq. 2. These methods are usually local in character and thus may require an extensive search over a large number of initial guesses to find all possible solutions. For biological systems, the search complexity can be reduced somewhat by taking advantage of the natural limits on the values of the state variables to bracket the region in the state space where the system is expected to operate and where the search needs to be carried out. More importantly, the dynamic models of biological systems often exhibit specific types of structure that arise from physical considerations and can thus be exploited in the computation of all the steady states using computational algorithms that have been developed in the literature. For example, if each component on the right-hand side of the system of ODEs in Eq. 1, f_i, involves linear combinations of rational functions of variables and parameters, then the algorithm developed in Zwolak et al.[40] can be used to find all the steady

Table 1. Parameter Values for the Cell Cycle Model in Eq. 4[43]

$k'_1 = 0.01$
$k'_{25} = 0.04$
$k''_{25} = 100$
$k_{INH} = 0.1$
$k_{CAK} = 1$

states (the algorithm converts the steady-state equations into a system of polynomial equations and uses a globally convergent homotopy method to find all the roots of the system of polynomials).

Most models of biological networks have linear combinations of rational functions for the right-hand side of their system of ODEs (see the cell-cycle and λ-switch models studied in the next two sections for examples). In fact, the right-hand sides are usually even more restricted to mass action and Michaelis–Menten type kinetics. Mass action kinetics have the form $k \times S_1 \times S_2 \times \cdots \times S_n$, where k is a rate constant (parameter) and S_i represents the concentration of a protein (variable). Michaelis–Menten kinetics have the form $k \times S \times E/(K_m + S)$, where k is a rate constant (parameter), K_m is a Michaelis constant (parameter), S is the substrate concentration (variable), and E is the enzyme concentration (variable). Clearly, these kinetics are rational functions. Once the target steady states are identified, the domains of attraction for each steady state can be computed. Then, the switching rule of Eq. 3 ensures a priori where the system will end up upon switching at a given point in the state space, provided that this point is within the domain of attraction of a stable steady state. Finally, it should be noted that even in the rare case that a structure cannot be identified—and subsequently not all of the steady states can be found—the proposed method still provides useful information regarding the feasibility of switching into any of the known steady states by verifying whether the state at any given time is contained within its domain of attraction.

Remark 2. The issue of robustness of the proposed approach with respect to model uncertainty can be explicitly handled by modifying the computation of the domains of attraction following the methodology proposed in El-Farra and Christofides[39] to account for the presence of parametric model uncertainty in the computation of the domain of attraction using bounds on the variation of the model parameters.

Remark 3. The Lyapunov function–based approach that we follow for the construction of the domains of attraction for the individual stable steady states yields a domain of attraction estimate that is dependent on the specific Lyapunov function used. To improve on the obtained estimate, one can use a group of different Lyapunov functions to come up with a larger estimate of the domain of attraction. Other methods for the construction of the Lyapunov function, such as Zubov's method[41] and the sum-of-squares decomposition approach,[42] can also be used. Acceptability of the computed estimates should ultimately be judged with respect to the size of the expected operating regime. Once the domain of attraction estimates are obtained, the switching rule of Eq. 3 ensures that the system will go to a certain stable steady state if the switching occurs at a point that is within the domain of attraction of this steady state. Finally, we note that the case of multiple mode switchings can be handled in a sequential fashion—the same way that the first mode switch is handled—by tracking where the state is at the time of each switch.

Remark 4. It should be noted that the proposed approach is not limited by the dimensionality of the system under consideration but applies to systems of any dimensionality. The estimation of the domain of attraction uses only simple algebraic computations and does not incur prohibitive computational costs with increasing dimensionality. In the simulation studies presented below, the domains of attraction are plotted for the sake of a visual demonstration. However, a plot of the domain of attraction is not *required* for the implementation of the switching rule, and thus poses no limitation when considering systems of higher dimensions. The knowledge of the domain of attraction is contained completely in the value of the level set c_i, obtained when computing the estimate of the domain of attraction. At the time of implementation, to ascertain whether the state is within the domain of attraction requires evaluating only the Lyapunov function and verifying whether $V_i(x(T)) \leq c_i$. To reduce the possible conservatism of the resulting estimate, it is often desirable to find the largest value of c_i for which the estimate $\Omega_{c_i} = \{x : V_i(x) \leq c_i\}$ is fully contained within Π_i. For this purpose, an iterative procedure to recompute (and enlarge) the estimate of the domain of attraction can be used whereby the value of c_i is gradually increased in each iteration until a value c_i^{max} is reached where for any $c_i > c_i^{max}$, Ω_{c_i} is no longer fully contained in Π_i. The level set $\Omega_{c_i}^{max}$ then is the largest estimate of the domain of attraction that can be obtained using the level sets of the given Lyapunov function. Note that, for a given value of c_i in each iteration, the determination of whether Ω_{c_i} is fully contained in Π_i involves only inexpensive algebraic computations and thus this iterative procedure does not incur prohibitive computational costs as the dimensionality of the system increases.

The same procedure also applies when a family of Lyapunov functions is used to estimate the domain of attraction of a given steady state. Finally, it should be noted that how close the obtained estimate is to the actual domain of attraction depends on the particular system structure as well as the method used to compute this estimate (in this case the particular Lyapunov functions chosen). In general, it is expected that the estimate will not capture the entire domain of attraction, which implies that the union of all the estimates of the domains of attraction

Table 2. Steady-State Values (u_s, v_s) for the Cell Cycle Model for Different Values of k'_2, k''_2, and k_{wee}

k'_2	k''_2	k_{wee}	Mode	M-Arrest State	G2-Arrest State	Reference
0.01	10	3.5	G2-arrest	n/a	(0.016, 0.802)	
0.01	0.5	2.0	M-arrest	(0.202, 0.329)	n/a	
0.015	0.1	3.5	Bistable	(0.276, 0.442)	(0.012, 0.666)	
0.01	10	2.0	Oscillatory	n/a	n/a	Figure 2b
0.01	10	2.5	Oscillatory	n/a	n/a	Figure 4

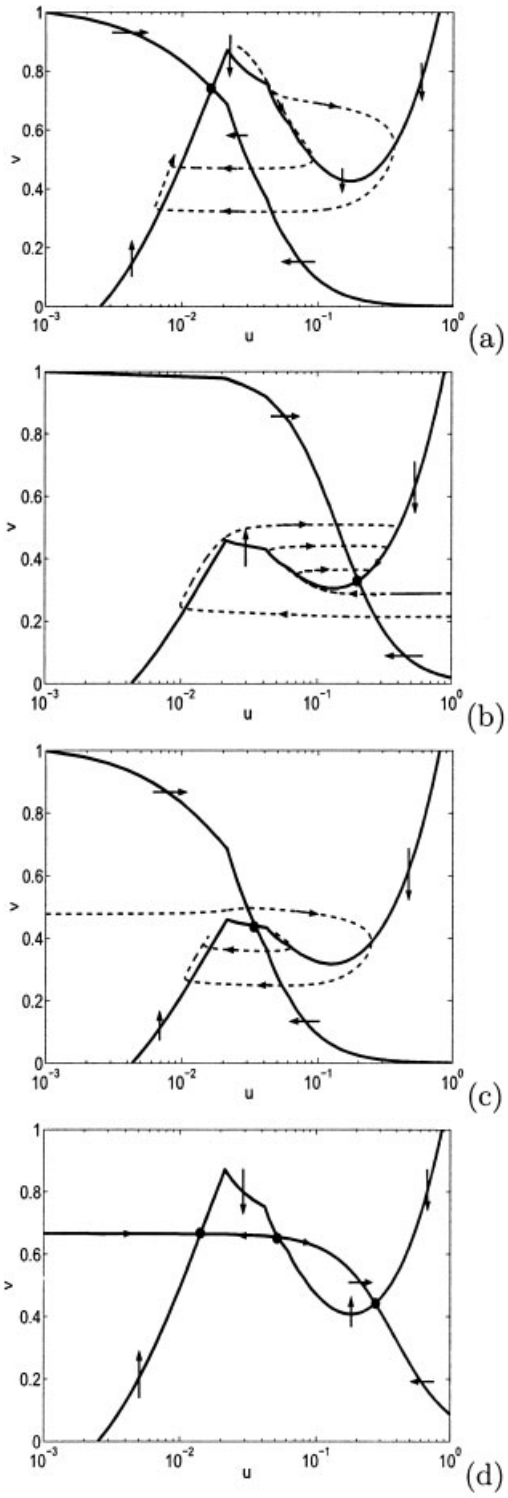

Figure 1. Phase-plane portraits of the system of Eq. 4, for different values of k_2', k_2'', and k_{wee}.

(a) Stable steady state with most MPF inactive, (b) stable steady state with most MPF active, (c) unstable steady state surrounded by a limit cycle, and (d) bistability: two stable steady states separated by an unstable saddle point.

of all the steady states will not cover the entire state space. An implication of this, for the case when switching of the network is controlled externally and a priori stability guarantees are sought, is that switching should be delayed until the state trajectory enters the computed estimate of the domain of attraction of the desired target steady state. The "gaps" between the different estimates (and thus the conservatism of the switching policy) can be reduced either with the help of dynamic simulations or by augmenting the individual estimates using any of the methods cited in Remark 3.

Remark 5. The proposed approach models biological networks using deterministic differential equations and does not account for possible network stochastic behavior. Such stochasticity can be modeled as uncertainty in the model parameters, and thus be handled directly by modifying the computation of the domains of attraction in a way that accounts explicitly for the effect of parameter model uncertainty following the methodology proposed in El-Farra and Christofides.[39]

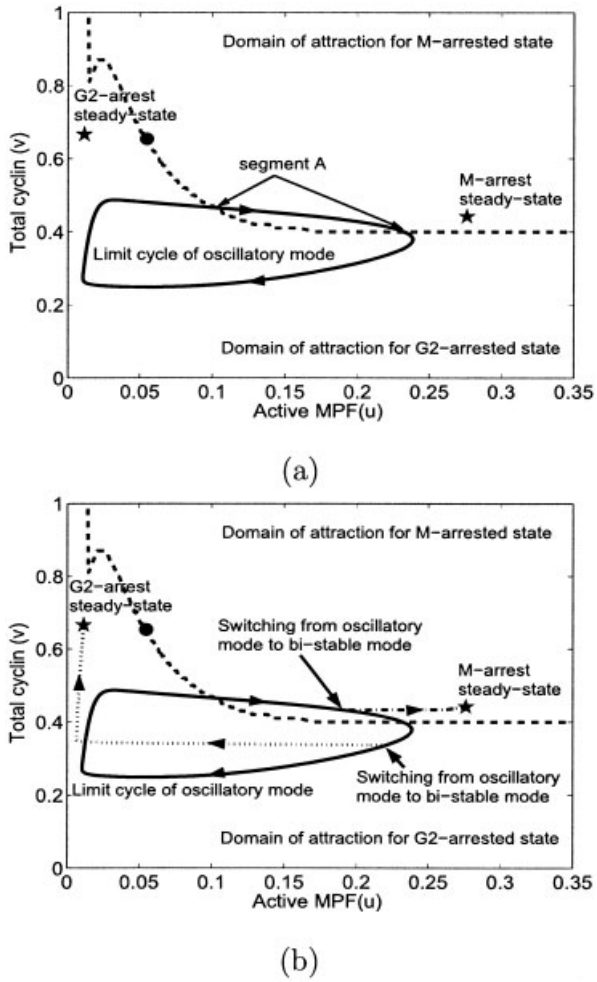

Figure 2. (a) Plot showing the overlap of the limit cycle of the oscillatory mode with the domains of attraction for the M-arrested steady state (entire area above dashed curve) and for the G2-arrested steady state (entire area below the dashed curve). (b) Plot showing that switching from the oscillatory to the bistable mode moves the system to different steady states depending on where switching takes place.

In both cases, the oscillatory mode is fixed at $k_2' = 0.01$, $k_2'' = 10$, $k_{wee} = 2.0$.

In the next two sections, we demonstrate, through computer simulations, the application of this methodology to the analysis of mode transitions in two biological networks, one arising in eukaryotic cell cycle regulation and the other in the bacteriophage λ-switch system. We note here that the focus in both examples is not on the modeling aspect, but rather on illustrating how the proposed analysis method can be applied given some available model of the network (which could come either from first principles or from data).

Application to Eukaryotic Cell Cycle Regulation

We consider here an example network of biochemical reactions, based on cyclin-dependent kinases and their associated proteins, which are involved in cell cycle control in frog egg development. A detailed description of this network is given in Novak and Tyson,[43] where the authors use standard principles

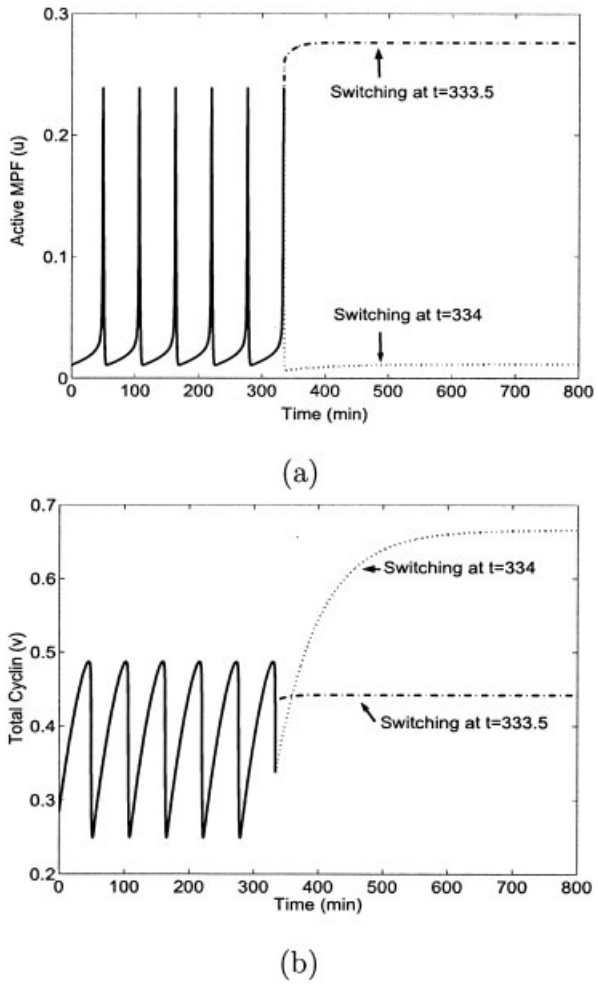

Figure 3. Time-evolution plots of (a) active MPF and (b) total cyclin upon switching from the oscillatory to the bistable mode at two representative switching times.

At $t = 333.5$ min, the state trajectory lies on segment A (see Figure 2a) and therefore switching lands the state in the M-arrested steady state (dash–dotted line), whereas at $t = 334$ min, switching lands the state in the G2-arrested steady state (dotted line). In both cases, the oscillatory mode is fixed at $k_2' = 0.01$, $k_2'' = 10$, $k_{wee} = 2.0$.

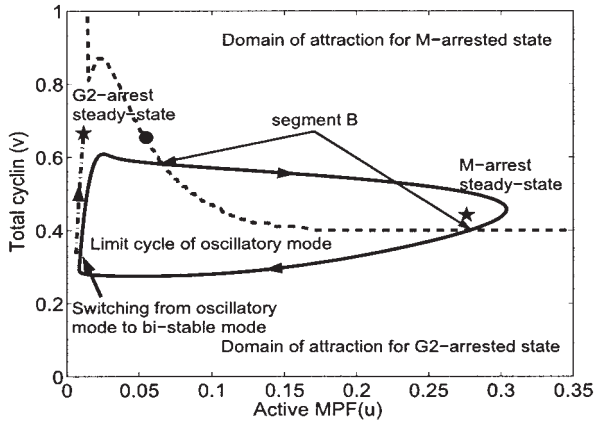

Figure 4. Plot showing that switching from the oscillatory mode (of the following parameter values: $k_2' = 0.01$, $k_2'' = 10$, $k_{wee} = 2.5$) to the bistable mode at the same time as in Figure 2b (t = 333.5 min) moves the system to G2-arrested steady state (instead of M-arrested steady state) because switching does not occur on segment B.

Note that the portion of the limit cycle overlapping the domain of attraction of the M-arrested steady state (segment B) is larger than the one in Figure 2a (segment A).

of biochemical kinetics and rate equations to construct a nonlinear dynamic model of the network that describes the time evolution of the key species including free cyclin, the M-phase promoting factor (MPF), and other regulatory enzymes. The model parameters have either been estimated from kinetic experiments in frog egg extracts or assigned values consistent with experimental observations. For illustration purposes, we will consider below the simplified network model derived by the authors (focusing only on the positive-feedback loops in the network), which captures the basic stages of frog egg development. The model is given by

$$\frac{du}{dt} = \frac{k_1'}{G} - (k_2' + k_2''u^2 + k_{wee})u + (k_{25}' + k_{25}''u^2)\left(\frac{v}{G} - u\right)$$
$$\frac{dv}{dt} = k_1' - (k_2' + k_2''u^2)v \qquad (4)$$

where $G = 1 + (k_{INH}/k_{CAK})$; k_{INH} is the rate constant for inhibition of INH, a protein that negatively regulates MPF; k_{CAK} is the rate constant for activation of CAK, a cdc2-activating kinase; u is a dimensionless concentration of active MPF and v is a dimensionless concentration of total cyclin; k_2' and k_2'' are rate constants for the low-activity and high-activity forms, respectively, of cyclin degradation; k_{25}' and k_{25}'' are rate constants for the low-activity and high-activity forms, respectively, of tyrosine dephosphorylation of MPF; k_1' is a rate constant for cyclin synthesis; k_{wee} is the rate constant for inhibition of *Wee1*, an enzyme responsible for the tyrosine phosphorylation of MPF (which inhibits MPF activity) (see Novak and Tyson[43] for model derivation from the molecular mechanism and Table 1 for the parameter values). Bifurcation and phase-plane analysis of the above model[43] shows that, by

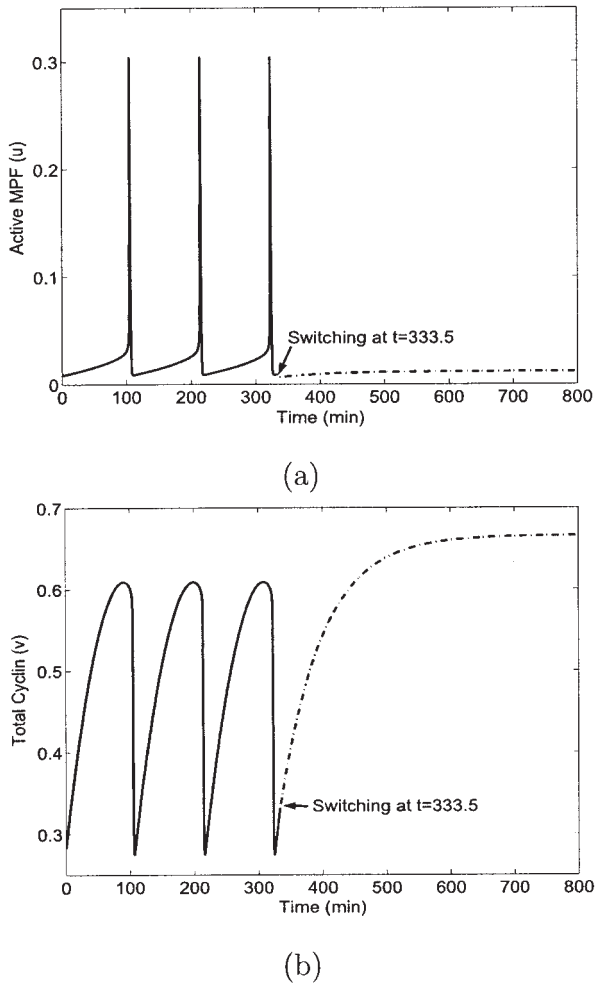

Figure 5. Time-evolution plots of (a) active MPF and (b) total cyclin upon switching from the oscillatory to the bistable mode at t = 333.5 min.

In both cases, the oscillatory mode is fixed at $k_2' = 0.01$, $k_2'' = 10$, $k_{wee} = 2.5$.

changing the values of k_2', k_2'', and k_{wee}, the following four modes of behavior are predicted (see Table 2):

(1) A G2-arrested state (blocked before the G2–M transition) characterized by high cyclin concentration and little MPF activity. This corresponds to a unique, asymptotically stable steady state ($k_2' = 0.01$, $k_2'' = 10$, $k_{\text{wee}} = 3.5$; see Figure 1a).

(2) An M-arrested state (blocked before the meta-to-anaphase transition) state with an abundance of active MPF. This corresponds to a unique, asymptotically stable steady state ($k_2' = 0.01$, $k_2'' = 0.5$, $k_{wee} = 2.0$; see Figure 1b).

(3) An oscillatory state (alternating phases of DNA synthesis and mitosis) exhibiting sustained, periodic fluctuation of MPF activity and total cyclin protein. This corresponds to a stable limit cycle surrounding an unstable equilibrium point ($k_2' = 0.01$, $k_2'' = 10$, $k_{wee} = 2.0$; see Figure 1c).

(4) Coexisting stable steady states of G2-arrest and M-arrest. This corresponds to three steady states: one unstable and two locally asymptotically stable ($k_2' = 0.015$, $k_2'' = 0.1$, $k_{wee} = 3.5$; see Figure 1d).

The above analysis predicts that slight increases in k_2' and k_{wee}, accompanied by a significant drop in k_2'' (which could be driven, for example, by downregulation of cyclin degradation), can induce a transition from the oscillatory mode of MPF activity (early embryo stage) to the bistable mode. However, it is not clear from this analysis alone whether the cell will end up in a G2- or an M-arrested state upon switching. To address this question, we initially compute the domains of attraction of both steady states in the bistable mode. This is done using a Lyapunov function of the form $V = (u - u_s)^4 + 10(v - v_s)^2$, where u_s and v_s are the steady-state values. The basic idea here is to compute, for each steady state, the region in the (u, v) space where the time derivative of V is negative-definite along the trajectories of the dynamical system of Eq. 4, and then use this region to obtain an estimate of the domain of attraction. Although several candidate functions could be used, this particular function was found to yield acceptable estimates of the domains of attraction in the sense that the region obtained for each steady state covered a distinct and large part of the operating range considered (the two regions were mostly separated from one another along the separatrix running through the three steady states, and their union covered the entire range) with little overlapping between the two regions occurring only in the vicinity of the two steady states. Computer simulations were then used to check the regions of overlap and determine which domain of attraction they were contained in.

The domains of attraction for both steady states are depicted in Figure 2a. The entire area above the dashed curve (the separatrix) is the domain of attraction of the M-arrested state, whereas the area below is the domain of attraction of the G2-arrested state. Both stable steady states are denoted by asterisks on the plot and the unstable steady state is denoted by a circle on the separatrix. By plotting the limit cycle (obtained from the oscillatory mode) on the same plot, we see that a portion of the limit cycle lies within the domain of attraction of the M-arrested steady state (segment A in Figure 2a), whereas the rest is completely within the domain of attraction of the G2-arrested steady state. Based on this analysis, we conclude that switching from the oscillatory mode to the bistable mode would move the cell to the G2-arrested state only if the transition occurs at times when the state is not on segment A,

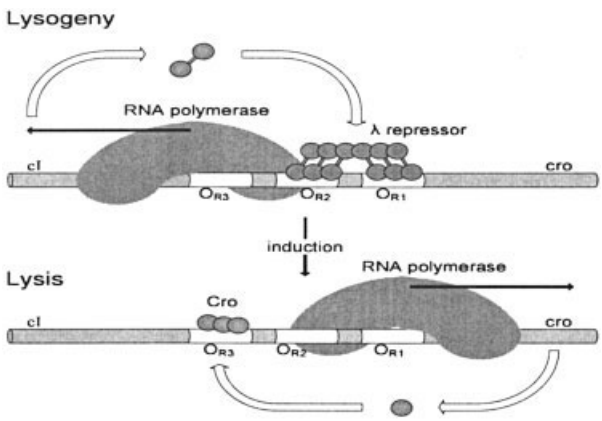

Figure 6. Schematic representation of the molecular mechanism responsible for the lysogenic to lytic mode transition in the bacteriophage λ.

Table 3. Parameter Values for the Bacteriophage λ Model in Eq. 5[15]

$\rho_y = 62.92$	$\beta_1 = 0.08$
$\alpha = 11$	$\beta_2 = 0.08$
$m_x = 1$	$\beta_3 = 0.08$
$m_y = 1$	$\beta_4 = 1$
$\sigma_1 = 2$	$\beta_5 = 1$
$\sigma_2 = 0.08$	

whereas it would end up in the M-arrested state if switching were to occur on segment A. This conclusion is verified by the dotted and dash–dotted state trajectories, respectively, shown in Figure 2b. The corresponding plots of the time evolution of the states in both switching scenarios are given in Figure 3 for two representative switching times. Note that, because of the periodic nature of the solution in the oscillatory mode, there are many time intervals, between $t = 0$ and $t = 333.5$ min, when the limit cycle trajectory is on segment A. These intervals are separated by one period of the limit cycle. Switching during any of these intervals to the bistable mode moves the system to the M-arrested state. Similarly, there are many time intervals when the trajectory is not on segment A. Switching during any of those intervals will land the system at the G2-arrested state.

Figure 4 shows the limit cycle resulting when the rate of inhibition of *Wee1* is increased to $k_{wee} = 2.5$ (with k_2' and k_2'' remaining fixed at 0.01 and 10, respectively). In a comparison with Figure 2a, we observe that a larger portion of the limit cycle (segment B in Figure 4) lies within the domain of attraction of the M-arrested steady state. Therefore, unlike the case of Figure 2a, when switching from the oscillatory mode to the bistable mode takes place at $t = 333.5$ min, the state is not within the domain of attraction of the M-arrested steady state. Switching in this case lands the system at the G2-arrested steady state. The corresponding time-evolution plots are given in Figure 5.

Application to the Bacteriophage λ-Switch System

We consider an example of a biological switch observed in the bacteriophage λ. An excellent review and detailed description of the molecular regulatory mechanisms in the bacteriophage λ-switch can be found in Ptashne.[14] Bacteriophage λ is a virus capable of infecting *Escherichia coli* bacteria. The virus attaches its tail to the surface of the host bacterium cell, drills a hole in the cell wall, and squirts its chromosome into the bacterium, leaving its coat behind. λ is an obligate parasite—it must inject its DNA into the bacterium to multiply. Upon infection, it can follow either one of two different pathways. First, the injected phage chromosome lysogenizes its host: all but one of the phage genes are turned off, and one phage chromosome, called prophage, becomes part of the host chromosome. As the lysogen (the bacterium bearing the prophage) grows and divides, the prophage is passively replicated and quiescently distributed to the progeny bacteria. Second, the phage chromosome enters the lytic mode: various sets of phage genes are turned on and off according to a precisely regulated program, the λ chromosome is extensively replicated, new head and tail proteins are synthesized, new phage particles are formed within bacterium, and some 45 min after the infection the bacterium lyses and releases about 100 progeny phage. Once the virus is in the lysogenic state, it can shift to the lysis state under certain conditions, such as whether the bacterial culture is irradiated with ultraviolet (UV) light.

The molecular regulatory mechanism responsible for the lysogeny/lysis decision is known as the *phage λ-switch* and the switch to lytic growth is called *induction*. A schematic representation of the λ-switch performance in the lysogenic and lytic steady states is shown in Figure 6.

To understand how the switch works, we need to consider two regulatory genes (*cI* and *cro*) and the regulatory region called O_R (right operator). In a lysogen, *cI* is on and *cro* is off, and vice versa when lytic growth ensues. The operator consists of three binding sites (O_{R1}, O_{R2}, and O_{R3}) that overlap two opposing promoters. One of these, P_R, directs transcription of lytic genes and the other, P_{RM}, directs transcription of the *cI* gene. In a lysogen, the λ repressor (the product of *cI* gene), at O_R, is bound at the two adjacent sites O_{R1} and O_{R2}. At these positions, it performs two functions: it represses rightward transcription from the promoter P_R, thereby turning off expression of *cro* and other lytic genes; simultaneously it activates transcription of its own gene from the promoter P_{RM}. Upon induction, repressor vacates the operator and transcription from P_R commences spontaneously. The first newly made protein is *Cro*. This protein binds first to O_{R3}, apparently helping to abolish repressor synthesis.

To illustrate the application of our methodology, we consider the following bacteriophage λ synthetic network model described in Hasty et al.[15] (other more detailed models can also be used):

$$\frac{dx}{dt} = \frac{m_x(1 + x^2 + \alpha\sigma_1 x^4)}{Q(x, y)} - \gamma_x x$$
$$\frac{dy}{dt} = \frac{m_y\rho_y(1 + y^2)}{Q(x, y)} - \gamma_y y \tag{5}$$

where

$$Q(x, y) = 1 + x^2 + \sigma_1 x^4 + \sigma_1\sigma_2 x^6 + y^2 + (\beta_1 + \beta_2)y^4 + \beta_1\beta_3 y^6 + \sigma_1\beta_4 x^4 y^2 + \beta_5 x^2 y^2 \tag{6}$$

Table 4. Steady-State Values (x_s, y_s) for the Lysogenic, Lytic, and Unstable Steady States for Different Values of γ_x and γ_y

γ_x	γ_y	Lysogenic State	Lytic State	Unstable State	Domain of Attraction
0.004	0.008	(32.39, 0)	(0, 16.22)	(2.79, 15.27)	Figures 8a, 14, 16a
0.05	0.008	(13.71, 0.01)	(0, 16.22)	(4.89, 6.38)	Figure 7
0.1	0.008	(10.75, 0.03)	(0, 16.22)	(5.37, 4.10)	Figures 8b, 16b
1	0.008	n/a	(0, 16.22)	n/a	
0.004	1	(32.39, 0)	n/a	n/a	
0.05	0.0005	(13.71, 0.11)	(0, 28.59)	(10.24, 3.47)	Figure 11a
0.05	0.06	(13.71, 0)	(0, 10.60)	(2.64, 7.65)	Figure 11b

Table 5. Lyapunov Functions Used in Estimating the Invariant Set $\Omega_{lysogenic}$ for the Lysogenic State and the Invariant Set Ω_{lytic} for the Lytic State

γ_x	γ_y	Lyapunov Function for $\Omega_{lysogenic}$	$c_{\max}$
0.004	0.008	$V = (x - x_s)^2 + (y - y_s)^2$	800
0.1	0.008	$V = (x - x_s)^2 + 0.6(y - y_s)^4$	100
0.05	0.0005	$V = (x - x_s)^2 + (y - y_s)^6$	150
0.05	0.06	$V = (x - x_s)^2 + 0.5(y - y_s)^2$	150
γ_x	γ_y	Lyapunov Function for Ω_{lytic}	$c_{\max}$
0.004	0.008	$V = 20(x - x_s)^2 + (y - y_s)^2$	100
0.1	0.008	$V = 0.5(x - x_s)^2 + (y - y_s)^2$	150
0.05	0.0005	$V = (x - x_s)^2 + 0.01(y - y_s)^4$	700
0.05	0.06	$V = 20(x - x_s)^2 + (y - y_s)^2$	100

and x and y represent dimensionless concentrations of the *CI* and *Cro* proteins, respectively; t represents dimensionless time; σ_1 and σ_2 are prefactors denoting the relative affinities for dimer binding to O_{R1} vs. that of binding to O_{R2} and O_{R3}, respectively; $\alpha > 1$ represents the degree to which transcription is enhanced by dimer occupation of O_{R2}; β_1–β_5 represent prefactors denoting binding strengths on reactions entailing the binding of *Cro* to different operator sites (see Eq. 17 in Hasty et al.[15]); the integers m_x and m_y represent the plasmid copy numbers for the two species; ρ_y represents a constant related to the scaling of y relative to x; γ_x and γ_y are directly proportional to the decay rates of *CI* and *Cro* proteins, respectively. The even polynomials in x occur as a result of dimerization and subsequent binding to the promoter region. The x^4 term represents the transcription when the two operator sites O_{R1} and O_{R2} are occupied (x^2x^2). The x^6 term represents the occupation of all three operator sites and arises in the denominator because dimer occupation of O_{R3} inhibits polymerase binding and shuts off transcription. The values of the model parameters in Eqs. 5 and 6 are given in Table 3. The steady-state values for different *CI* and *Cro* degradation rates are given in Table 4.

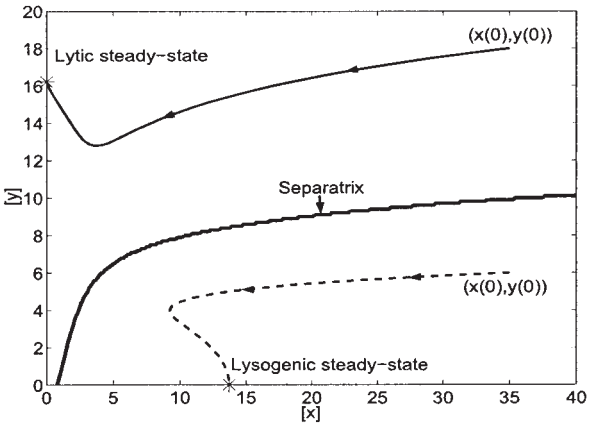

Figure 7. Phase plot for the moderate CI degradation mode showing that an initial condition within the lysogenic domain of attraction (entire area below the separatrix) will converge to the lysogenic steady state (dashed trajectory) and that an initial condition within the lytic domain of attraction (entire area above the separatrix) will converge to the lytic steady state (solid trajectory).

Here, the *Cro* degradation rate is fixed at $\gamma_y = 0.008$.

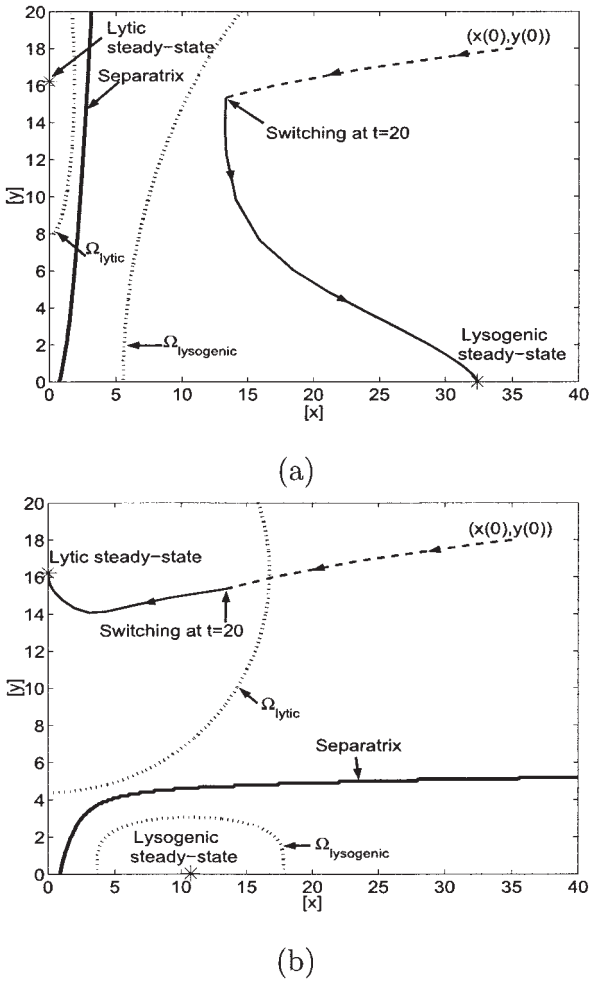

Figure 8. Phase plot showing the system of Eq. 5 being initialized using $\gamma_x = 0.05$ (dashed trajectory) and undergoing: (a) a decrease in the degradation rate of *CI* protein (to $\gamma_x = 0.004$) at $t = 20$, leading the state to converge to the lysogenic steady state, and (b) an increase in the degradation rate of *CI* protein (to $\gamma_x = 0.1$) at $t = 20$, leading the state to converge to the lytic steady state.

In both cases, the *Cro* degradation rate is fixed at $\gamma_y = 0.008$.

Bifurcation and phase-plane analysis of the above model show that, by changing the values of γ_x and γ_y, the system of Eq. 5 can exhibit one of the following modes of behavior:

- A mode with a single globally asymptotically stable equilibrium point corresponding to the lysogenic steady state (low γ_x and high γ_y).
- A mode with a single globally asymptotically stable equilibrium point corresponding to the lytic steady state (high γ_x and low γ_y).
- A bistable mode where the stable lysogenic and lytic steady states coexist together with a third unstable steady state.

Note from Table 4 that for a fixed γ_y, as the degradation rate of protein *CI* is increased (larger γ_x value), the lysogenic steady

state keeps shifting to smaller concentrations until the system exhibits only the lytic steady state (the lysogenic steady state vanishes). By contrast, for a fixed γ_x, when the degradation rate of protein *Cro* is increased (larger γ_y value), the lytic steady state keeps shifting to smaller concentrations until the system exhibits only the lysogenic steady state (the lytic steady state vanishes).

Focusing on the bistable mode, we initially compute estimates of the domains of attraction of both steady states for different values of the *CI* and *Cro* protein degradation rate. Because of the complex nonlinearity of the system—relative to that of the cell cycle model—the Lyapunov function used in the cell cycle example did not yield good estimates of the domain of attraction for the λ-switch system. However, we were able to attain "conservative" estimates of the domains of attraction using several other polynomial Lyapunov functions that are listed in Table 5. For each steady state, we initially used the corresponding V to determine the region Π, where $\dot{V} < 0$ and

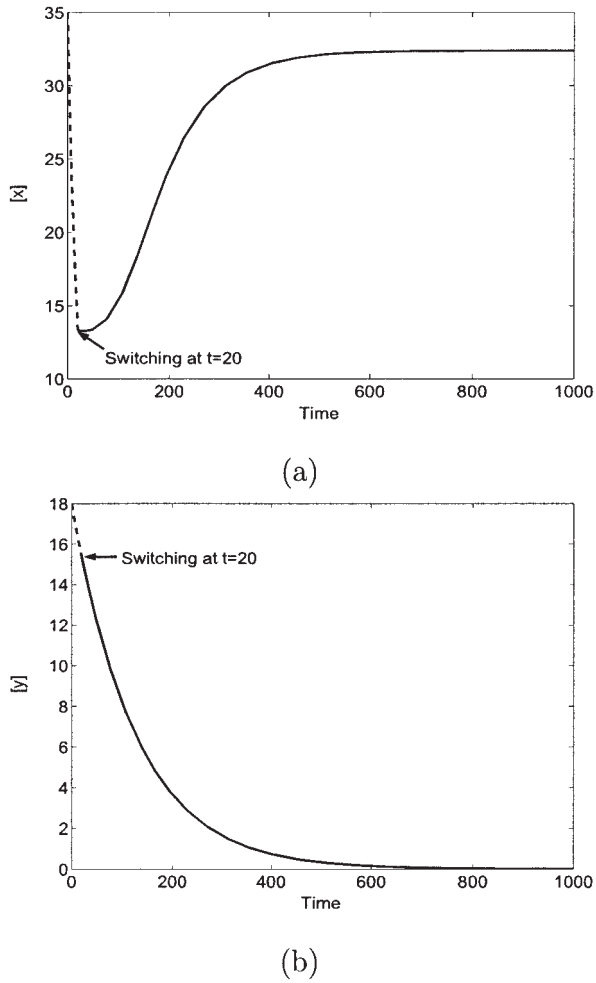

Figure 9. Time-evolution plots of the (a) *CI* and (b) *Cro* protein concentrations when the system undergoes a transition from the $\gamma_x = 0.05$ mode (dashed lines) to the $\gamma_x = 0.004$ mode at $t = 20$ and converges (solid lines) to the lysogenic steady state.

The *Cro* degradation rate is fixed at $\gamma_y = 0.008$.

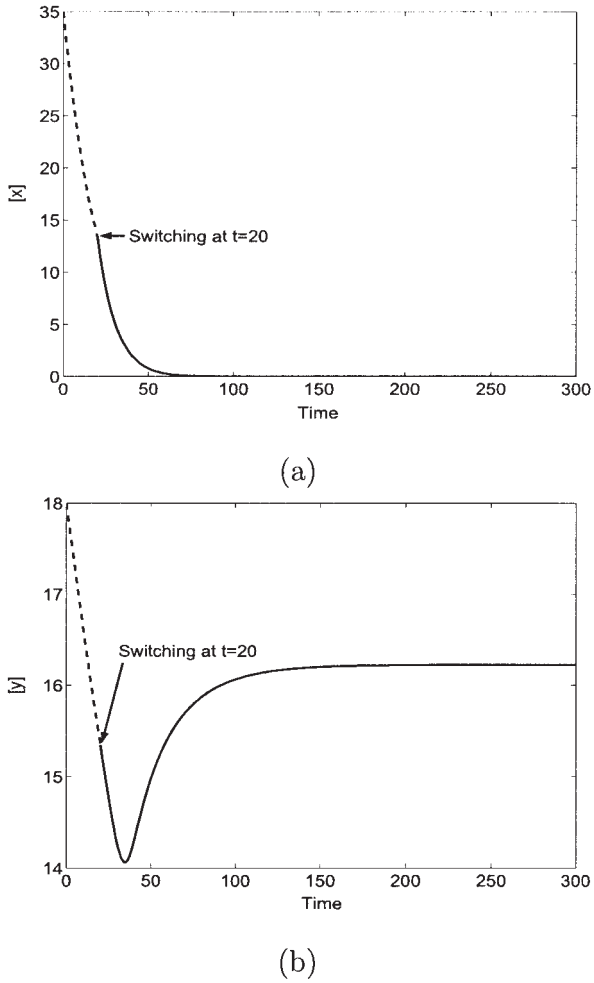

Figure 10. Time-evolution plots of the (a) *CI* and (b) *Cro* protein concentrations when the system undergoes a transition from the $\gamma_x = 0.05$ mode (dashed lines) to the $\gamma_x = 0.1$ mode at $t = 20$ and converges (solid lines) to the lytic steady state.

The *Cro* degradation rate is fixed at $\gamma_y = 0.008$.

then constructed an invariant set (a level set) within this region, $\Omega = \{x : V(x) \leq c_{max}\}$, where c_{max} is a positive constant for which Ω is contained in Π. The boundaries of the invariant sets, $\Omega_{lysogenic}$ and Ω_{lytic}, are depicted by the dotted lines in Figures 8, 11, 14, and 16 for the lysogenic state and lytic state (note that, for each level set, only the part that is contained within the given x–y range is shown). To get an idea of the possible conservatism of these estimates, we also used computer simulations to compare, for each steady state, the entire domain of attraction (separated by the separatrix) with the estimate provided by the corresponding level set.

Figures 7, 8a, and 8b show the domains of attraction for the lysogenic and lytic steady states for: (1) a moderate *CI* degradation rate ($\gamma_x = 0.05$, $\gamma_y = 0.008$), (2) a relatively low *CI* degradation rate ($\gamma_x = 0.004$, $\gamma_y = 0.008$), and (3) a relatively high *CI* degradation rate ($\gamma_x = 0.1$, $\gamma_y = 0.008$), respectively, keeping the *Cro* protein degradation rate constant. Figures 7, 11a, and 11b show the domains of attraction for the lysogenic

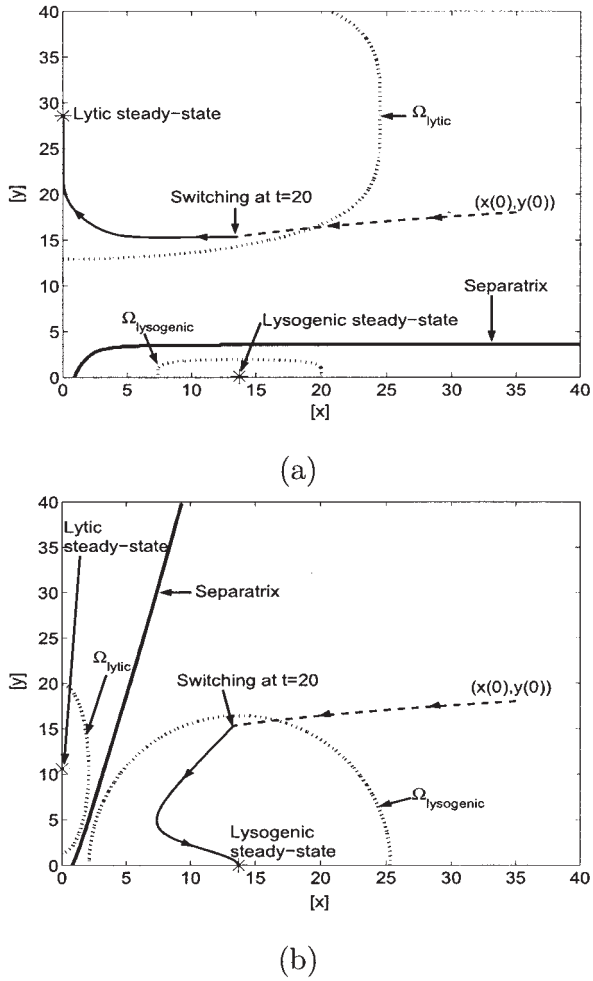

Figure 11. Phase plot showing the system of Eq. 5 being initialized using $\gamma_y = 0.008$ (dashed trajectory) and undergoing: (a) a decrease in the degradation rate of *Cro* protein (to $\gamma_y = 0.0005$) at $t = 20$, leading the state to converge to the lytic steady state, and (b) an increase in the degradation rate of *Cro* protein (to $\gamma_y = 0.06$) at $t = 20$, leading the state to converge to the lysogenic steady state.

In both cases, the *CI* degradation rate is fixed at $\gamma_x = 0.05$.

and lytic steady states for: (1) a moderate *Cro* degradation rate ($\gamma_x = 0.05$, $\gamma_y = 0.008$), (2) a relatively low *Cro* degradation rate ($\gamma_x = 0.05$, $\gamma_y = 0.0005$), and (3) a relatively high *Cro* degradation rate ($\gamma_x = 0.05$, $\gamma_y = 0.06$), respectively, keeping the *CI* protein degradation rate constant. The entire area below (or to the right of) the separatrix is the entire domain of attraction for the lysogenic steady state, whereas the area above (or to the left of) the separatrix is the entire domain of attraction for the lytic steady state. Both stable steady states are denoted by asterisks on each plot.

It is clear from the plots that an increase in the *CI* degradation rate results in a smaller domain of attraction for the lysogenic state (and a larger one for the lytic state) and vice versa. In the limiting case of very high degradation rates, the lysogenic state vanishes and the domain of attraction of the lytic state occupies the entire state space (single globally asymptotically stable equilibrium point). The opposite trend is observed when the *Cro* protein degradation rate is increased. In particular, increasing γ_y leads to a smaller domain of attraction for the lytic state and a larger one for the lysogenic state. For very high *Cro* degradation rates, the lytic steady state vanishes and the domain of attraction for the lysogenic state turns into the entire state space.

Therefore, in the bistable mode, the initial condition plays a critical role in deciding which steady state the bacteriophage λ will attain. Also, the size of the domain of attraction for each state helps explain why the lysogenic state is more likely to be observed under a given set of conditions,[16] whereas the lytic state is more likely to be seen under a different set of conditions. Figure 7 shows that starting from an initial condition of high *CI* and *Cro* concentrations, the phage ends up in the lytic state because the initial condition is within its domain of

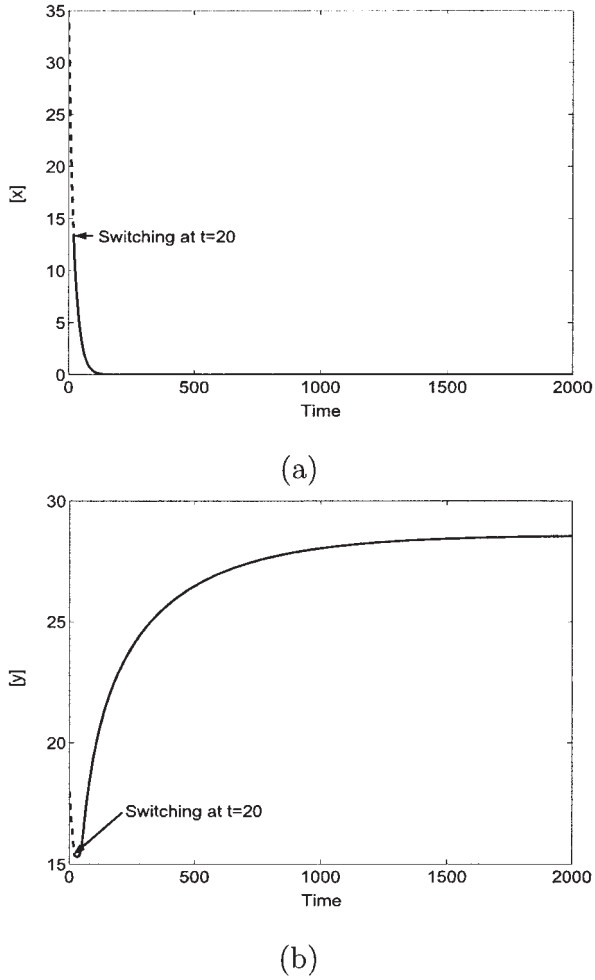

Figure 12. Time-evolution plots of the (a) *CI* and (b) *Cro* protein concentrations when the system initialized at $[x(0), y(0)] = (35, 18)$ undergoes a transition from the $\gamma_y = 0.008$ mode (dashed lines) to the $\gamma_y = 0.0005$ mode at $t = 20$ and converges (solid lines) to the lytic steady state.

The *CI* degradation rate is fixed at $\gamma_x = 0.05$.

attraction (solid trajectory). Initializing the system, however, at high *CI* but low *Cro* concentrations drives the phage to the lysogenic state (dashed trajectory).

We now demonstrate the effect of switching in the *CI* protein degradation rate on whether the bacteriophage will exhibit the lytic or lysogenic steady state. To this end, we initialize the system within the moderate *CI* degradation mode ($\gamma_x = 0.05$, $\gamma_y = 0.008$) at the initial condition $[x(0), y(0)] = (35, 18)$ and allow it to evolve in this mode until, at $t = 20$, a mode transition is enforced (see dashed trajectories in Figures 8a and 8b). The results show that, for a fixed transition time, depending on which mode is being switched in, the phage takes a different path. For example, Figure 8a shows that when the system switches to the relatively low *CI* degradation mode ($\gamma_x = 0.004$, $\gamma_y = 0.008$) at $t = 20$, the system state is within the invariant set of the lysogenic steady state ($\Omega_{lysogenic}$) and thus the phage ends up with lysogeny. Figure 8b, on the other hand,

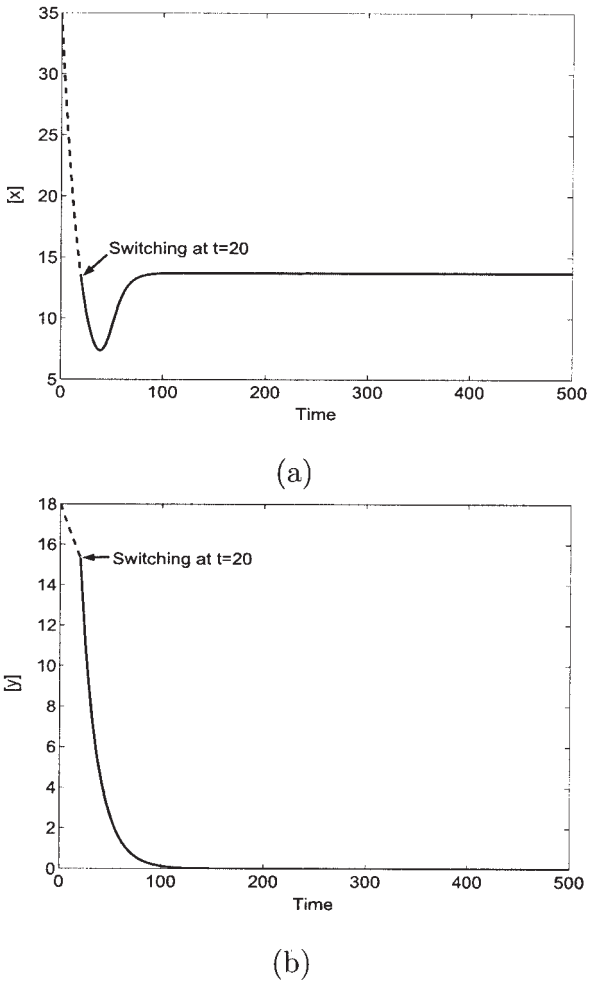

Figure 13. Time-evolution plots of the (a) *CI* and (b) *Cro* protein concentrations when the system initialized at $[x(0), y(0)] = (35, 18)$ undergoes a transition from the $\gamma_y = 0.008$ mode (dashed lines) to the $\gamma_y = 0.06$ mode at $t = 20$ and converges (solid lines) to the lysogenic steady state.

The *CI* degradation rate is fixed at $\gamma_x = 0.05$.

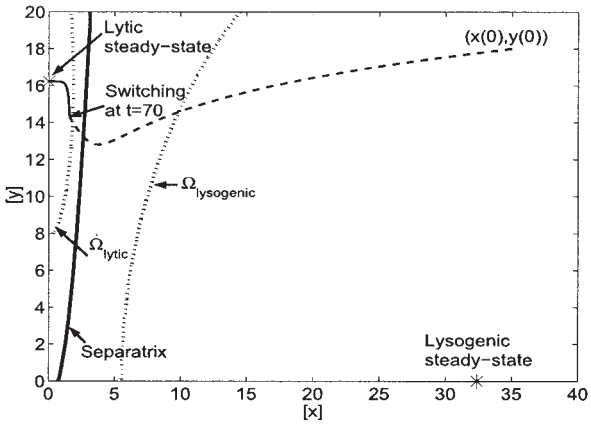

Figure 14. Phase plot showing the system undergoing a transition from the $\gamma_x = 0.05$ mode (dashed trajectory) to the $\gamma_x = 0.004$ at $t = 70$ and converging (solid trajectory) to the lytic steady state.

The *Cro* degradation rate is fixed at $\gamma_y = 0.008$.

shows that when the relatively high *CI* degradation mode ($\gamma_x = 0.1$, $\gamma_y = 0.008$) is switched in at $t = 20$, the system state is within the invariant set of the lytic steady state (Ω_{lytic}) and thus the phage ends up with lysis instead. The time-evolution plots for both scenarios are depicted in Figures 9 and 10, respectively.

Figure 8b gives some insight into the implications of using a conservative estimate of the domain of attraction as the basis for switching, in lieu of the true domain of attraction (which could be more computationally expensive to obtain). In particular, if the relatively high *CI* degradation mode ($\gamma_x = 0.1$, $\gamma_y = 0.008$) is switched in before the states enter the invariant set of the lytic state Ω_{lytic}, then, having no knowledge about what the actual domain of attraction looks like, the only conclusion we would be able to make is that there is no guarantee that the phage would end up in the lytic state if switching were to take place at such a time. Switching has to be "delayed" until the state enters Ω_{lytic} to guarantee that the phage would end up with lysis.

To demonstrate the effect of switching in the *Cro* protein degradation rate, the system is initialized within the moderate *Cro* degradation mode ($\gamma_x = 0.05$, $\gamma_y = 0.008$) at the same initial condition $[x(0), y(0)] = (35, 18)$ and allowed to evolve in this mode until, at $t = 20$, a mode transition is enforced (see dashed trajectories in Figures 11a and 11b). The results show that, for a fixed transition time, depending on which mode is being switched in, the phage takes a different path. For example, Figure 11a shows that when the system switches to the relatively low *Cro* degradation mode ($\gamma_x = 0.05$, $\gamma_y = 0.0005$) at $t = 20$, the system state is within Ω_{lytic} and thus the phage ends up with lysis. Figure 11b, on the other hand, shows that when the relatively high *Cro* degradation mode ($\gamma_x = 0.05$, $\gamma_y = 0.06$) is switched in at $t = 20$, the system state is within $\Omega_{lysogenic}$ and thus the phage ends up with lysogeny instead. The time-evolution plots for both scenarios are depicted in Figures 12 and 13, respectively.

So far in our analysis, we have fixed the transition time and showed that which mode is activated at that time determines

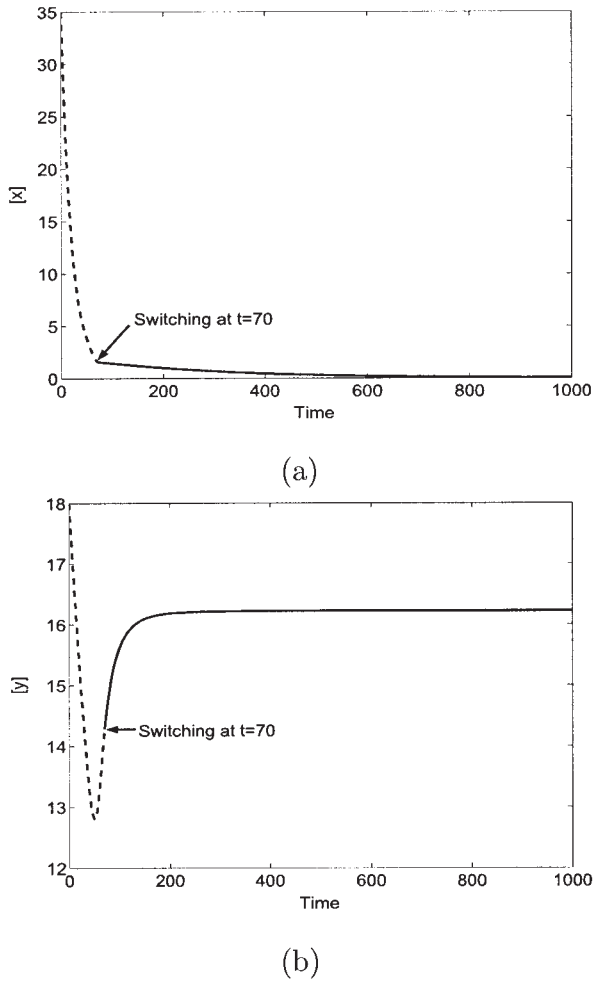

Figure 15. Time-evolution plots of the (a) *CI* and (b) *Cro* protein concentrations when the system undergoes a transition from the $\gamma_x = 0.05$ mode (dashed lines) to the $\gamma_x = 0.004$ mode at $t = 70$ and converges (solid lines) to the lytic steady state.

The *Cro* degradation rate is fixed at $\gamma_y = 0.008$.

the final state of the phage. Here, we demonstrate the effect of varying the transition time, for a given mode transition, on the steady-state behavior of the phage. To this end, we reconsider the switching scenario presented in Figure 8a, where the system switches from the moderate ($\gamma_x = 0.05$) to the relatively low ($\gamma_x = 0.004$) *CI* degradation mode and the *Cro* degradation rate is fixed at $\gamma_y = 0.008$. However, instead of carrying out the transition at $t = 20$ as in Figure 8a, the switch is delayed until $t = 70$. The result is depicted in Figure 14, which shows that at $t = 70$, the system state is within the invariant set of the lytic steady state (Ω_{lytic}) and thus the phage ends up with lysis. The corresponding time-evolution plots are given in Figure 15. By comparing Figure 8a with Figure 14, we conclude that an early transition from moderate to relatively low *CI* degradation rate favors lysogeny, whereas a late transition favors lysis.

In the last simulation run, we demonstrate the effect of the initial condition on the outcome of switching for a given transition time. To this end, we initialize the system within the moderate *CI* degradation mode ($\gamma_x = 0.05$, $\gamma_y = 0.008$) at an initial condition different from the one considered in Figure 8 and characterized by high concentration of *CI* and low concentration of *Cro* [$x(0) = 35$, $y(0) = 2$]. We allow the system to evolve in this mode until, at $t = 40$, a mode transition is enforced (see dashed trajectories in Figures 16a and 16b). The results show that, for a fixed transition time, switching close to a particular steady state will converge to that particular steady state, independently of which mode is being switched in. For example, Figure 16a shows that when the system switches to the relatively low *CI* degradation mode ($\gamma_x = 0.004$, $\gamma_y = 0.008$) at $t = 40$, the state is within the invariant set of the lysogenic steady state ($\Omega_{lysogenic}$) and thus the phage ends up with lysogeny. Similarly, Figure 16b shows that when the relatively high *CI* degradation mode ($\gamma_x = 0.1$, $\gamma_y = 0.008$) is

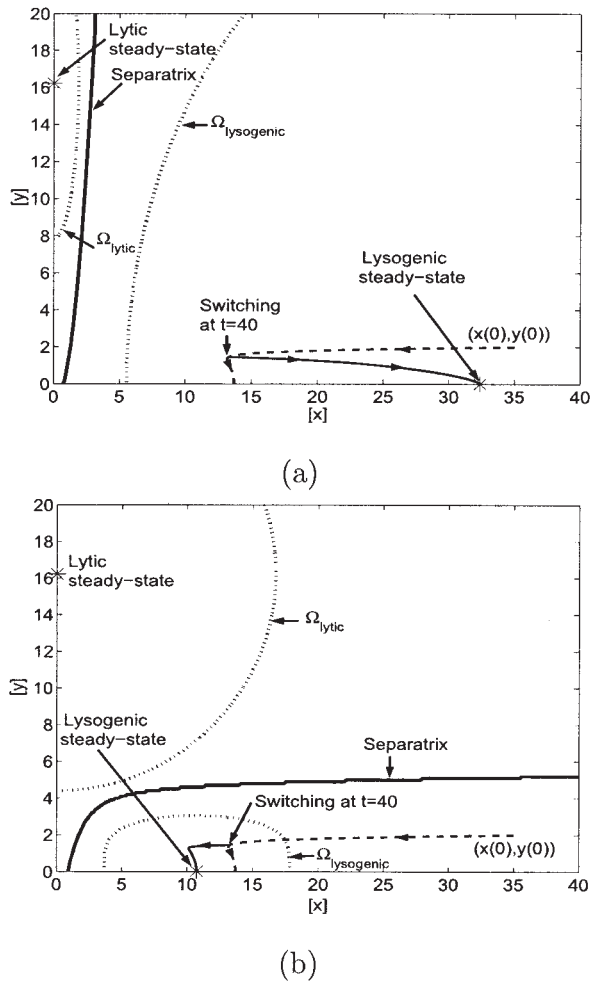

Figure 16. Phase plot showing the system of Eq. 5 being initialized using $\gamma_x = 0.05$ (dashed trajectory) and undergoing: (a) a decrease in the degradation rate of *CI* protein (to $\gamma_x = 0.004$) at $t = 40$ and (b) an increase in the degradation rate of *CI* protein (to $\gamma_x = 0.1$) at $t = 40$, both leading the state to converge to the lysogenic steady state.

In both cases, the *Cro* degradation rate is fixed at $\gamma_y = 0.008$.

switched in at $t = 40$, the state is again within the invariant set of the lysogenic steady state ($\Omega_{lysogenic}$) and thus the phage ends up with lysogeny (albeit with a smaller steady-state concentration of *CI* protein). The time-evolution plots for both scenarios are depicted in Figures 17 and 18, respectively. Note that this result is different from that obtained in Figure 8 where the final steady-state behavior is dependent on which mode is being switched in. The difference lies in the fact that the system state at the switching time considered in Figure 16 is contained within the invariant set of the lysogenic steady state ($\Omega_{lysogenic}$) for both the low and high *CI* degradation modes, and thus only the lysogenic steady state can be observed regardless of whether the low or high *CI* degradation mode is activated.

Conclusions

In this work, a methodology for the analysis of mode transitions in biological networks was presented. The proposed approach was predicated on the notion of orchestrating switching between the domains of attraction of the steady states of the constituent modes. The proposed method was demonstrated using models of biological networks that arise in cell cycle regulation and the bacteriophage λ-switch system. The proposed approach has implications both for understanding the outcome of naturally occurring mode transitions and for the ability to manipulate network behavior by enforcing mode transitions.

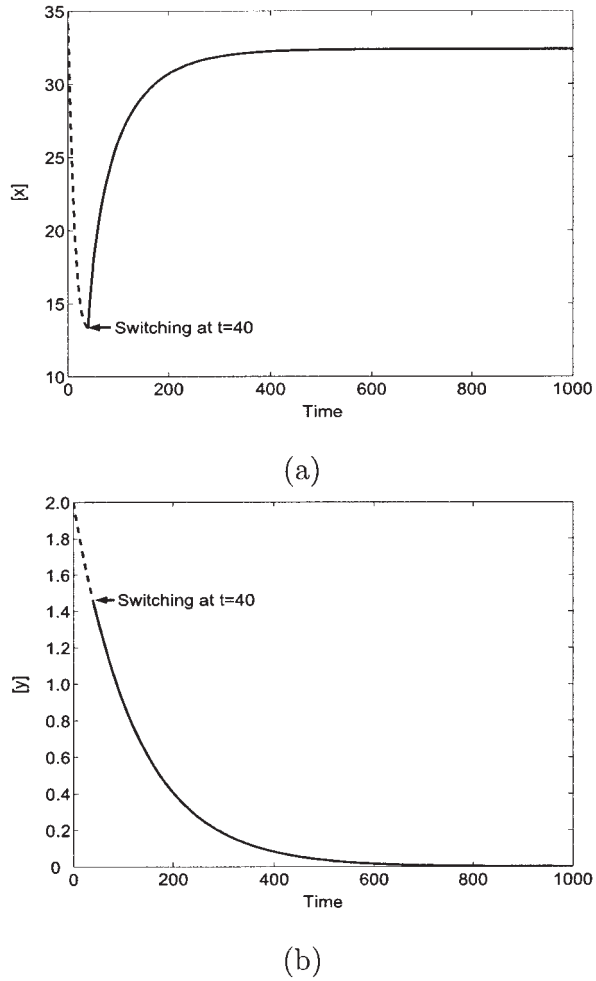

Figure 17. Time-evolution plots of the (a) *CI* and (b) *Cro* protein concentrations when the system initialized at [$x(0)$, $y(0)$] = (35, 2) undergoes a transition from the $\gamma_x = 0.05$ mode (dashed lines) to the $\gamma_x = 0.004$ mode at $t = 40$ and converges (solid lines) to the lytic steady state.

The *Cro* degradation rate is fixed at $\gamma_y = 0.008$.

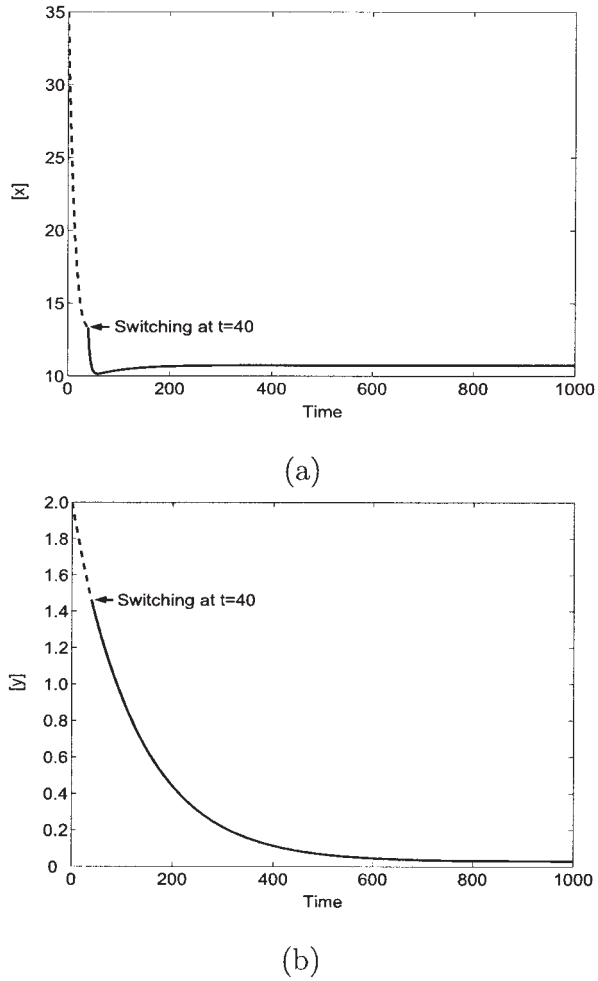

Figure 18. Time-evolution plots of the (a) *CI* and (b) *Cro* protein concentrations when the system initialized at [$x(0)$, $y(0)$] = (35, 2) undergoes a transition from the $\gamma_x = 0.05$ mode (dashed lines) to the $\gamma_x = 0.1$ mode at $t = 40$ and converges (solid lines) to the lytic steady state.

The *Cro* degradation rate is fixed at $\gamma_y = 0.008$.

Acknowledgments

Financial support from the National Science Foundation (Grant CTS-0129571) is gratefully acknowledged.

Literature Cited

1. Wiley HS, Shvartsman SY, Lauffenburger DA. Computational modeling of the EGF-receptor system: A paradigm for systems biology. *Trends Cell Biol*. 2003;13:43-50.

2. McAdams HH, Arkin A. Simulation of prokaryotic genetic circuits. *Ann Rev Biophys Biomol Struct*. 1998;27:199-224.
3. Smolen P, Baxter DA, Byrne JH. Modeling transcriptional control in gene networks: Methods, recent results, and future directions. *Bull Math Biol*. 2000;62:247-292.
4. De Jong H. Modeling and simulation of genetic regulatory systems: A literature review. *J Comput Biol*. 2002;9:67-103.
5. Bailey JE. Mathematical modeling and analysis in biochemical engineering: Past accomplishments and future opportunities. *Biotechnol Prog*. 1998;14:8-20.
6. Giersch C. Mathematical modelling of metabolism. *Curr Opin Plant Biol*. 2000;3:249-253.
7. Endy D, Brent R. Modelling cellular behavior. *Nature*. 2001;409:391-395.
8. Dasika MS, Gupta A, Maranas CD. A mixed integer linear programming (MILP) framework for inferring time delay in gene regulatory networks. Proc of Pacific Symposium on Biocomputing, Hawaii, HI; 2004:474-485.
9. Mendes P, Kell D. Non-linear optimization of biochemical pathways: Applications to metabolic engineering and parameter estimation. *Bioinformatics*. 1998;14:869-883.
10. Feng XJ, Rabitz H. Optimal identification of biochemical reaction networks. *Biophys J*. 2004;86:1270-1281.
11. Hasty J, McMillen D, Isaacs F, Collins JJ. Computational studies of gene regulatory networks: In numero molecular biology. *Nat Rev Genet*. 2001;2:268-279.
12. Tyson JJ, Chen K, Novak B. Network dynamics and cell physiology. *Nat Rev Mol Cell Biol*. 2001;2:908-916.
13. Alm E, Arkin AP. Biological networks. *Curr Opin Struct Biol*. 2003; 13:193-202.
14. Ptashne M. *A Genetic Switch: Gene Control and Phage* λ. Cambridge, MA: Cell Press; 1986.
15. Hasty J, Isaacs F, Dolnik M, McMillen D, Collins JJ. Designer gene networks: Towards fundamental cellular control. *Chaos*. 2001;11:207-220.
16. Santillán M, Mackey MC. Why the lysogenic state of phage λ is so stable: A mathematical modeling approach. *Biophys J*. 2004;86:75-84.
17. Hatzimanikatis V, Lee KH, Bailey JE. A mathematical description of regulation of the G1-S transition of the mammalian cell cycle. *Biotechnol Bioeng*. 1999;65:631-637.
18. Lewin B. *Genes VII*. Cambridge, UK: Oxford Univ. Press; 2000.
19. Tyson JJ, Csikasz-Nagy A, Novak B. The dynamics of cell cycle regulation. *BioEssays*. 2002;24:1095-1109.
20. Ghosh R, Tomlin CJ. Lateral inhibition through delta-notch signaling: A piecewise affine hybrid model. In: Di Benedetto MD, Sangiovanni-Vincentelli A, eds. *Lecture Notes in Computer Science Series*. Vol. 2034. Berlin, Germany: Springer-Verlag; 2001:232-246.
21. Alur R, Belta C, Kumar V, Mintz M, Pappas GJ, Rubin H, Schug J. Modeling and analyzing biomolecular networks. *Comput Sci Eng*. 2002;4:20-31.
22. Alur R, Belta C, Ivancic F, Kumar V, Mintz M, Pappas G, Rubin H, Schug J. Hybrid modeling and simulation of biomolecular networks. In: Di Benedetto MD, Sangiovanni-Vincentelli A, eds. *Lecture Notes in Computer Science Series*. Vol. 2034. Berlin, Germany: Springer-Verlag; 2001:19-32.
23. Yamalidou EC, Kantor J. Modeling and optimal control of discrete-event chemical processes using petri nets. *Comput Chem Eng*. 1990; 15:503-519.
24. Barton PI, Pantelides CC. Modeling of combined discrete/continuous processes. *AIChE J*. 1994;40:966-979.
25. Turkay M, Grossmann IE. Logic-based MINLP algorithms for the optimal synthesis of process networks. *Comput Chem Eng*. 1996;20: 959-978.
26. Vecchietti A, Grossmann IE. LOGMIP: A disjunctive 0-1 nonlinear optimizer for process systems models. *Comput Chem Eng*. 1997;21: S427-S432.
27. Grossmann IE, van den Heever SA, Harjukoski I. Discrete optimization methods and their role in the integration of planning and scheduling. Proc of 6th International Conference on Chemical Process Control, Tucson, AZ; 2001:124-152.
28. Hespanha J, Morse AS. Stability of switched systems with average dwell time. Proc of 38th IEEE Conference on Decision and Control, Phoenix, AZ; 1999:2655-2660.
29. Liberzon D, Morse AS. Basic problems in stability and design of switched systems. *IEEE Control Syst Mag*. 1999;19:59-70.
30. DeCarlo RA, Branicky MS, Petterson S, Lennartson B. Perspectives and results on the stability and stabilizability of hybrid systems. *Proc IEEE*. 2000;88:1069-1082.
31. Branicky MS, Mitter SK. Algorithms for optimal hybrid control. Proc of the 34th IEEE Conference on Decision and Control, New Orleans, LA; 1995:2661-2666.
32. Bemporad A, Morari M. Control of systems integrating logic, dynamics and constraints. *Automatica*. 1999;35:407-427.
33. Koutsoukos XD, Antsaklis PJ, Stiver JA, Lemmon MD. Supervisory control of hybrid systems. *Proc IEEE*. 2000;88:1026-1049.
34. Zhang P, Cassandras CG. An improved forward algorithm for optimal control of a class of hybrid systems. *IEEE Trans Autom Control*. 2002;47:1735-1739.
35. El-Farra NH, Christofides PD. Coordinating feedback and switching for control of hybrid nonlinear processes. *AIChE J*. 2003;49:2079-2098.
36. El-Farra NH, Christofides PD. Switching and feedback laws for control of constrained switched nonlinear systems. In: Tomlin CJ, Greenstreet MR, eds. *Lecture Notes in Computer Science Series*. Vol. 2289. Berlin, Germany: Springer-Verlag; 2002:164-178.
37. Khalil HK. *Nonlinear Systems*. 2nd Edition. New York, NY: Macmillan; 1996.
38. El-Farra NH, Christofides PD. Bounded robust control of constrained multivariable nonlinear processes. *Chem Eng Sci*. 2003;58:3025-3047.
39. El-Farra NH, Christofides PD. Integrating robustness, optimality and constraints in control of nonlinear processes. *Chem Eng Sci*. 2001;56: 1841-1868.
40. Zwolak JW, Tyson JJ, Watson LT. Finding all steady state solutions of chemical kinetic models. *Nonlinear Anal Real World Appl*. 2004;5: 801-814.
41. Dubljević S, Kazantzis N. A new Lyapunov design approach for nonlinear systems based on Zubov's method. *Automatica*. 2002;38: 1999-2007.
42. Papachristodoulou A, Prajna S, Doyle JC. On the construction of Lyapunov functions using the sum of squares decomposition. Proc of 41st IEEE Conference on Decision and Control, Las Vegas, NV; 2002:3482-3487.
43. Novak B, Tyson JJ. Modeling the cell division cycle: M-phase trigger, oscillations and size control. *J Theor Biol*. 1993;165:101-134.

Manuscript received Apr. 9, 2004, and revision received Dec. 26, 2004.